International Journal of Engineering and Advanced Technology Studies
Vol.7 No.2,Pp.1-24, November 2019
Published by ECRTD-UK
Print ISSN: 2053-5783(Print), Online ISSN: 2053-5791(online)

USING MODIFIED NANO- HYDROXYAPATITE FOR REMOVING IRON IONS CONTAMINANTS FROM GROUNDWATER

MD.Zunaud Siddiki Mamoon[1],Omar Al Maimun[2]
Lecturer, Civil Engineering, Rangpur Engineering Institute, Bangladesh
Researcher, Hydrology and Water Resources, Hohai University, Nanjing, China.

ABSTRACT: *In this article, concentrate about altered nano-hydroxyapatite (HAp) by nano-manganese oxide (Mn3O4) as adsorbent material to expel iron particles from ground-water. Various parameters were concentrated to choice ideal states of evacuating, for example, contact time, pH, beginning fixation, a measurement of adsorbent, disturbance speed and temperature. Energy studies included first request (R2 = 0.95), pseudo-first-request (R2 = 0.936), second-request (R2 = 0.98), pseudo-second-request (R2 = 0.99), Elovich condition model (R2 = 0.97), intraparticle dissemination (R2 = 0.96), Natarajan and Khalaf (R2 = 0.91) were completed, the acquired outcomes uncovered that the pseudo-second-request is the best to portray the adsorption procedure on the grounds that the connection coefficient is moving toward one (R2 = 0.95). Adsorption isotherm was determined by utilizing Freundlich, Langmuir and Temkin constants, adsorption limit from the Langmuir model was 0.606 mg/g. Thermodynamic parameters (ΔG, H = −55 KJ/mol, and S = −152 (KJ/mol)) for the adsorption procedure were additionally determined and talked about.*

KEYWORDS: Groundwater, Adsorption, Nano Materials, Hydroxyapatite, Manganese Oxide, Iron Ions, Kinetic, Thermodynamic

INTRODUCTION

Groundwater is an important resource for the livelihoods and food security of billions of people. It is one of the most difficult problems that pollute the groundwater and the presence of iron. Therefore, in this article, we try to find a solution to the problems of iron in the groundwater [1] [2].Among the appropriate solutions to remove or reduce the proportion of iron in the groundwater is Ion exchange [3], Reverse osmosis [4], Chemical precipi-tation [5], Electrolysis [6] and Adsorption [7], the choice of which depends upon the type and concentration of both sorptive material and sorbent employed, as well as their costs [8]

Among these, the adsorption method is more commonly used, adsorption is an effective technology to remove different contaminated from aqueous solu-tions. In this process, a very high rate of adsorption and excretion occurs. The simple function has caused this method to be one of the best ways to remove iron ions from groundwater such as Polyvinyl alcohol was used for removal of bromothymol blue and methylene blue from [9]. Removal of natural organic matter and its constituents from water by metal oxides and hydroxides based adsorbents were investigated [10]. Fluoride removal capacity from drinking wa-ter by Adsorption using nano-sized Alumina and Zirconia modified Alumina was tested [11]. Removal of Cu(II) and Zn(II) by unmodified Lignocellulosic Fibrous Layer of Palm Tree Trunk-Single was studied [12]. Removal of Cu(II) ions from water by rice husk (S.E. Abd Elhafez *et al.* 2016) [13], Pb (II), La (III), and Ag (I) ions was removed from aqueous solutions using mediated cellulose nanofibers [14]. Adsorptive of ibuprofen and diclofenac from water using met-al-organic framework-derived porous carbon was investigated [15]. Removal of Cr(VI) by a free metal material containing only C, N and O, and having envi-ronmental friendliness, was studied [16]. Removal of benzotriazole and benzi-midazole from water over a Co-based metal azolate framework MAF-5(Co) was investigated [17].

In this work, we have used modified nano hydroxyapatite by (Mn3O4) nano-particles to remove the iron ions from water by adsorption; parameters such as contact time, pH, adsorbent dosage, stirring speed and temperature were inves-tigated. Kinetic, Isotherm Adsorption and Thermodynamic parameters (ΔG,H, and$S$) for adsorption process were also calculated and discussed.

MATERIALS AND METHODS

Apparatus

We had all the measurements of pH using Misura Line 1010 pH meter (Roma-nia). All samples are stirred and heated by multiple Heating Magnetic Stirrer (VELP Scientifica) during experimental procedures as well, as micropipette (100-1000 μL) is also used. Spectrophotometer Instruments (CECIL3021), Brand (Cambridge, England). Determine the iron ions by Phenanthroline method. The samples were first mixed with KBr and then pressed into pellets. X-ray powder diffraction (XRD) data were collected at room temperature using a Philips 1710 Diffractometer. The patterns were run with Cu target and Ni filter (λ = 1.5418A˚) at 40 KV and 30 mA in the range of 2θ, with a scanning speed of 06 deg/s. Fourier transform infrared spectroscopy (FTIR) data were collected using a Per-kin-Elmer spectrometer model 1430 in the wave number range from 4000 to 400 cm−1 Examination on the TEM: Samples were examined by carbon coated grids with a JEOL 1010 Transmission Electron Microscope, made in Japan, at the Re-gional Center for Mycology and Biotechnology (RCMB), Al-Azhar University.

Procedures

Synthesis of Hydroxyapatite (HAp)

We have prepared HAp powder using the titration between both H3PO4, adwic 85% in burette and CaCl2·2H2O, Sigma-Aldrich, 99% - 103% in a beaker until adjustment the pH at a value of 10. Through the addition of NH4OH solution (adwic 30%) during the mixing process using a hotplate for heating the reaction mixture and stirring according to the following equation:

10CaCl2·2H2O+6H3PO4 + 20NH4OH → Ca10(PO4)6(OH)2
+ 20NH4Cl + 38H2O (I)

The mixture was heated in a microwave oven for 10 min until completely dryness and formation the precipitate, and then it was washed with distilled wa-ter and filtrated. The precipitate dried by microwave for 4 min [18].

Synthesis of Manganese Oxide

We can manufacture nano-manganese oxide (Mn3O4) by oxidation of MnCl2 solution with a concentrated H2O2 solution, followed by the addition of an NH3 aq. solution. The suspension thus obtained was treated at 90˚C [19]. With mi-crowave for 7 mint to dryness and formation the precipitate, then it was washed with distilled water and filtrated. The precipitate dried by microwave for 3 min.

Synthesis of Modified Hydroxyapatite Manganese Hydroxide (HApMn)

We have been able to prepare three modifications to test the removal of iron ions first (0.04 HAp:0.06 Mn3O4) second (0.06 HAp:0.04 Mn3O4) and the third (0.08 HAp:0.02 Mn3O4). The percentage of removing iron ions were (R%) = 49%, 47%, and 30% respectively. We chose (0.06 HAp:0.04 Mn3O4) R% = 47% and have found that the best modification is. Three composed of Modification of HAp by Mn3O4 were prepared and exam to remove iron ions, to complete this study.

Analytical Methods

Amount of adsorbent of iron on happening at any time (*qt*) was calculated as follows [8] [9]:

$$q_t = (C_o - C_t) V / m \qquad (1)$$

where, *Co* and *Ct* are the concentrations of iron ions at initial and equilibrium time, respectively (mg/L), *V* is the solution volume (L) and m is the mass of dry adsorbent used (g). At equilibrium, *qe* = *qt* and *Ct* = *Ce*; therefore, the amount of

sorbed metal ion (*qe*) was calculated according to Equation (2)

$$q_e = (C_o - C_e) V / m \qquad (2)$$

The removal efficiency (RE%) is calculated according to the following equa-tion [12]:

$$RE\% = (C_o - C_e) / C_o \times 100 \qquad (3)$$

RESULTS AND DISCUSSION

Characterizations

Figure 1(a) shows the FTIR (Fourier transform infrared spectroscopy) of HAp. The broad bands in the regions 1600 - 1700 cm−1 and 3200 - 3600 cm−1 corres-pond to H-O-H bands of lattice water. The bands characteristics of the phosphate and hydrogen phosphate groups in apatite environment are observed at 565, 632, 603, 962, and 1000 - 1100 cm−1 for $PO^3{}_4^-$ and at 875 cm−1 for $HPO^2{}_4^-$ [18]. FTIR of the Manganese Oxide sample is shown in **Figure 1(b)**. Several ab-sorption bands can be observed at 500 - 1000 cm−1 for (Mn-O), 3000 - 3500 cm−1 stretching, the 1636. While the 606, 564, 510.2 and 417 cm−1 bands should be as-cribed to the Mn–O vibrations in MnO6 octahedral [19]. FTIR results indicate the presence of some bounded water to HApMn.

Figure 2(a) and **Figure 2(b)** shows XRD (X-ray Diffraction) patterns of th

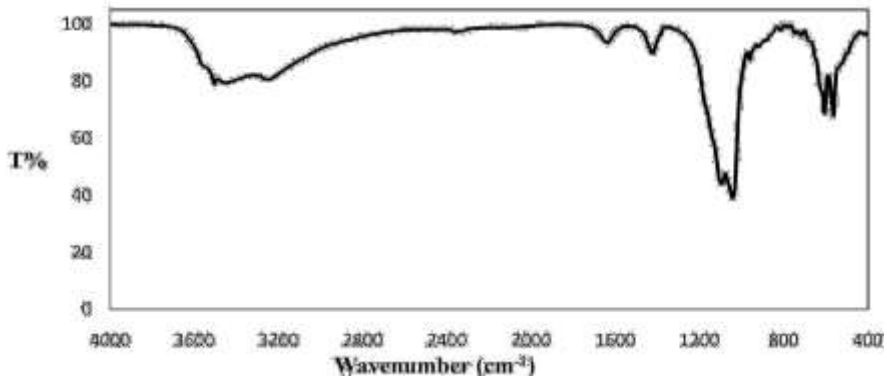

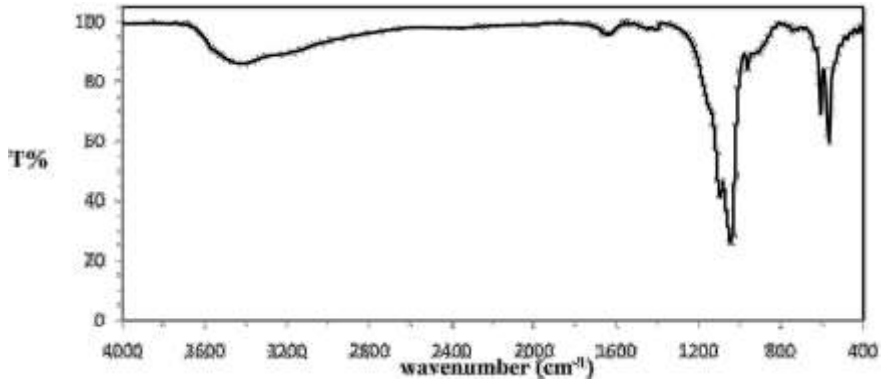

Figure 1. FTIR spectra for (a) HAp and (b) HApMn.

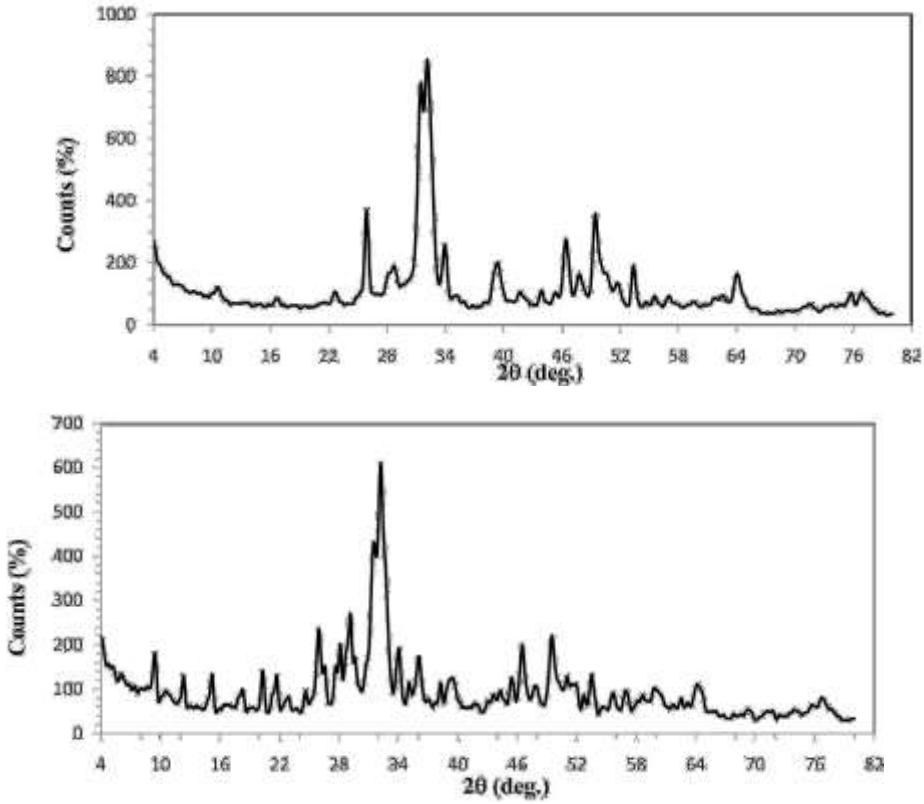

Figure 2. (a) XRD profiles for prepared HAp; (b) XRD profiles for Mn3O4.

HAp and Mn3O4 samples, respectively. The intensive diffraction peaks appeared at 25.9, 28.9, 31, 32.3, 33, 33.9, 36.9, 39.2, 44.3, 46.4, 47.8, 49.5, 51.22, 53.4, 58.4, 60.2, 64.5, 74.4, 76.7 and 55.9 are assigned to the characteristic peaks for Mn-O, and the peaks occurred at respectively, should be ascribed to the characteristic peaks for Mn-O [19]. Hence, the sample appears to be composed of a majority of HApMn. Scherer equation can be written as [7] [20]:

$$D \square K\lambda \beta \cos\theta \qquad (4)$$

where D is the crystal size (nm), λ is the wavelength of X-ray light, β is the full width of the half maximum of the diffraction peak, and θ is the diffraction angle. Shape factor of K is usually taken as 0.9. It was found that the particle sizes were 4.2 nm and 3.6 nm for HAp and Mn3O4, respectively. The result is tabulated in **Table 1**.

Figure 3(a) and **Figure 3(b)** show TEM (Transmission electron microscopy) of HAp profiles and Mn3O4 profiles respectively.

Study of Adsorption Factors

We have used a Patch method for all adsorption work, 100 ml of sample (2- 10) ppm, temperature (25 - 75)˚C, pH (3 - 8), contact time (5 - 90) min, the speed of agitation (100 - 8000) rpm, iron ions concentration was measured before placing

Table 1. Size of HAp and Mn3O4 calculate by XRD (Scherer equation) and measured by TEM.

Calculate by Scherer equation (XRD)			From TEM	
HAp	**Mn3O4**		**HAp**	**Mn3O4**
Distance	**Distance**	**Statistical Function**	**Distance**	**Distance**
nm	**Nm**	**Base Unit**	nm	Nm
22.62	8.91	**Count**	5	5
26.38	9.09	**Mean**	23.58	9.20
18.66	11.52	**Minimum**	18.66	8.14
28.42	8.34	**Maximum**	28.42	11.52
21.79	8.14	**Standard Deviation**	3.86	1.35
		Cal. by XRD	4.2	3.6

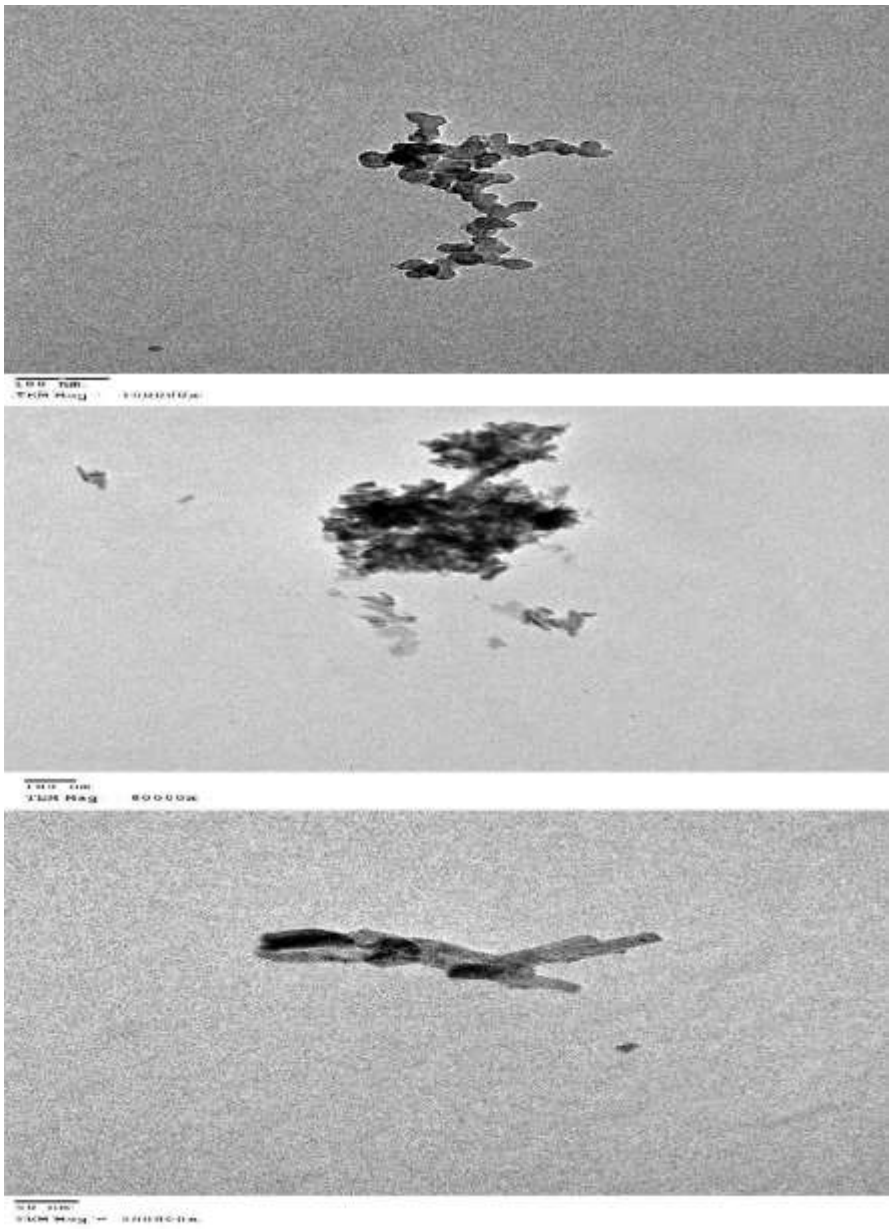

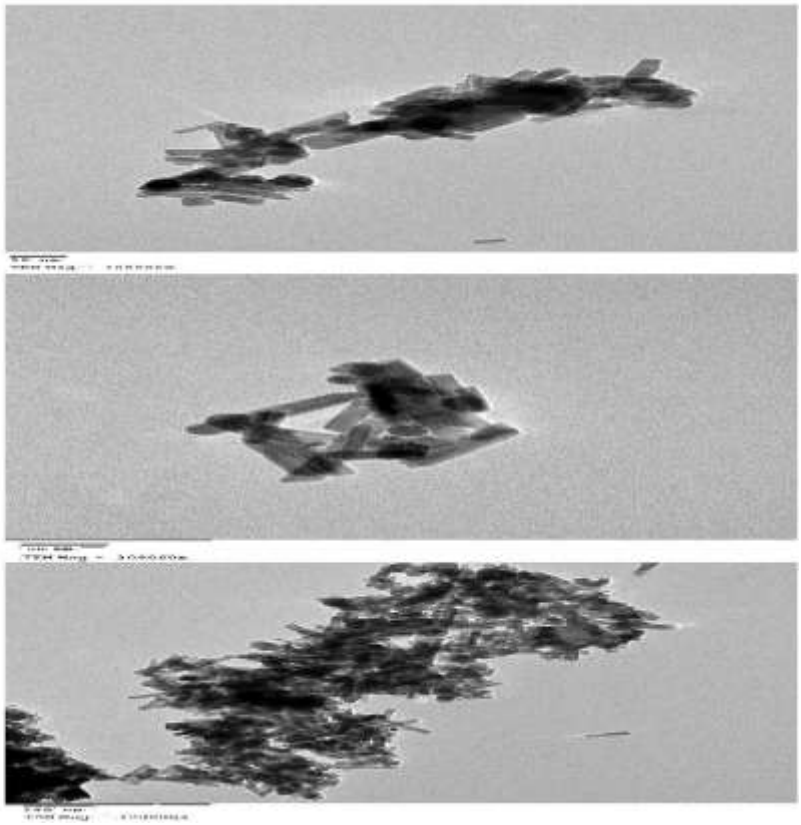

Figure 3. (a) TEM profiles for prepared of HAp; (b) TEM profiles for prepared Mn3O4.

The adsorbent and after putting them for different samples obtained from dif-ferent wells as shown in **Table 2**. Various adsorption parameters for the effective removal of iron ions using modified hydroxyapatite as an adsorbent from aqueous solution were studied and optimized.

Effect of Contact Time

We have studied the effect of contact time in different time periods ranging from 5 to 90 min with the initial metal concentration of 2 ppm iron ions in presence 0.1 g of HApMn with continuous stirring at 400 rpm and at pH 6 [21]. Remove iron ions over time, where it was about 25% in 5 minutes and reached 60% in 90 minutes see **Figure 4**.

Effect of pH

PH is an important factor in the adsorption process. The pH of 3 - 8 is determine

Table 2. Iron ion concentrations of well samples before and after treatment.

no	Place (well name)	well name	Before Ppm	After Ppm
1	**New Awolad Khalf**	3	0.94	0.22
2	**New Awolad Khalf**	4	1.03	0.23
3	**New Awolad Khalf**	5	1.1	0.24
4	**Arab Elataiat south**	2	0.68	0.155
5	**Old Elkhamima**	3	0.58	0.12

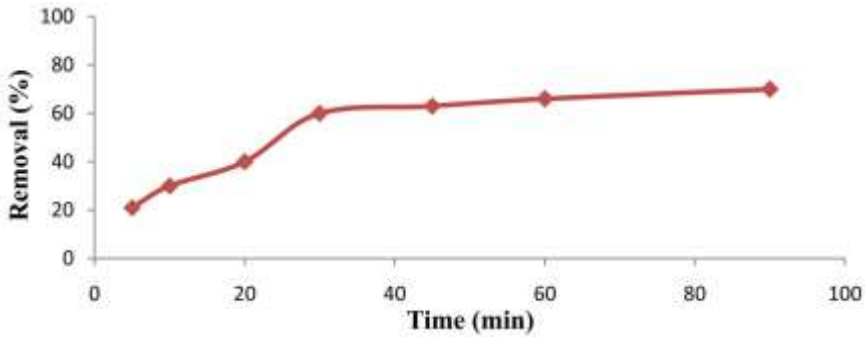

Figure 4. Effect of contact time on iron ions removal using HApMn.

By using 30% ammonia solution or 37% hydrochloric acid solution and the same conditions as above. Note that the increase in pH increases the removal iron ions (see **Figure 5**). It may be due to precipitation of iron ions as Fe+3 hydroxide brown precipitate [22].

Effect of Agitation Speed

The effect of the stirring speed on the removal of iron ions under the same expe-rimental conditions is studied by agitation Speed (100 - 800) rpm. The efficiency of the removal was found to increase with increased agitation speed (see **Figure 6**). Iron ions increase the speed of stirring [23].

Effect of Initial Concentration of Iron Ions

By studying the effect of iron ion concentration per 100 ml, we found that the removal efficiency was reduced by increasing the concentration of iron per 100 ml see **Figure 7** [24].

Effect of Temperature

Under the same experimental conditions the effect of temperature on iron ions removal was studied by varying the temperature from 25˚C to 75˚C. As we see from **Figure 8**, as the temperature increases the removal percentage increase [25].

Applications of the Method

Around 100 ml of sample (well water) at pH about 7.4, the temperature at 30˚C, stirring at 400 rpm, stirring time 30 min was used to measure iron ions concentrations.

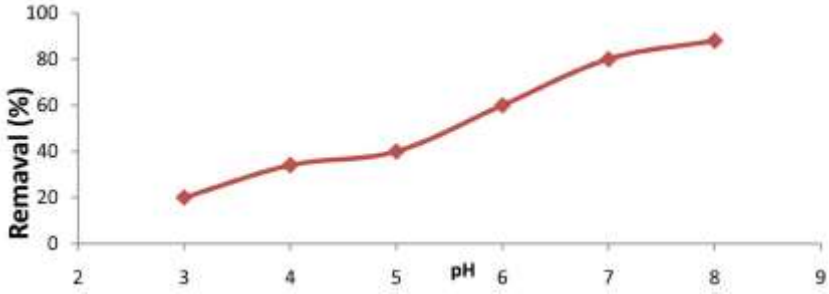

Figure 5. Effect of pH on iron ions removal using HApMn

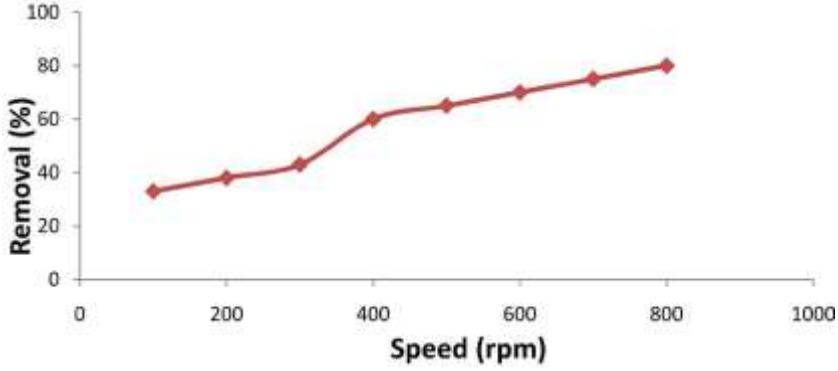

Figure 6. Effect of agitation speed on iron ions removal using HApMn.

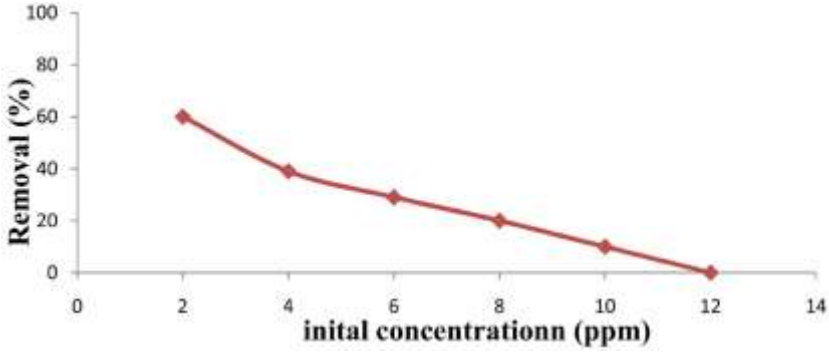

Figure 7. Effect of initial concentration on iron ions removal using HApMn.

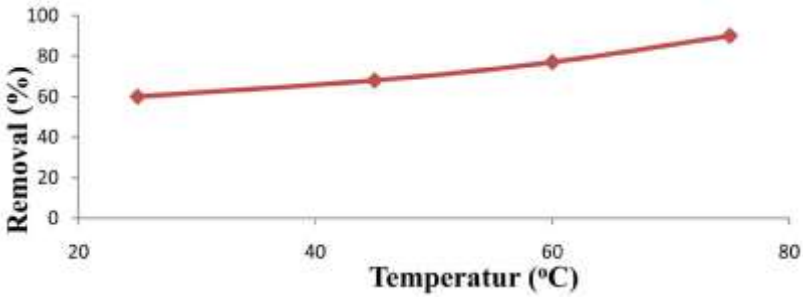

Figure 8. Effect of temperature on iron ions removal using HApMn.

Kinetics Modeling

We have done a study the kinetic of adsorption and adsorption rate controls; we found a metal ion uptake rate with a residence time of adsorb ate uptake at solid interface solution. We have studied seven equations models, the first-order rate equation, pseudo-first order rate equation, second-order rate equation, pseudo-second order rate equation, intra-particle diffusion, and Elovich equations. See **Table 3** for the parameter values.

First Order Kinetic Equation

The equation of a straight line is applicable [12] [26]:

$$-\ln \left(C_t / C_o\right) = K_1 t \qquad (5)$$

where, Ct (mg/L) is the concentration at a given time t and Co (mg/L) is initial concentration of iron ions in solution. $K1$ (min−1) is the first order rate constant. The regression $R2$ obtained by the linear plot of –ln(Ct/Co) against t (**Figure 9**), is shown in **Table 3**, $R2$ was greater than 0.9, which indicates a good fit to the ex-perimental data.

Second Order Kinetic Equation

The linear version is given by this relationship [12] [26]:

$$\left(1/C_t\right) - \left(1/C_o\right) = K_2 t\,. \qquad (6)$$

where, $k2$ [L/mg/min] is the second order rate constant for the adsorption process, determined from the linear plot of (1/Ct – 1/Co) against t, shown in (**Figure 10**) for iron ions. See **Table 3**, for the value of the constants. The

Table 3. Summary of kinetic modeling parameters.

No	Kinetics model	Parameters	Value
1	First-order rate equation	***K*1 (min^{-1})**	0.0116
	$-\ln(Ct/Co) = K1t$	R^2	0.915
2	Second order rate equation	***K*2 (L/mg·min)**	0.013
	$[1/Ct] - [1/Co] = K2t$	R^2	0.948
3	Lagergren pseudo first-order equation.	***K*1 (min^{-1})**	−0.018
	$\mathrm{Ln}\,(qe - qt) = \ln qe - K1t$	R^2	0.936
4	Pseudo second-order rate equation	***K*2 (g/mg·min)**	0.036
	$t\ q_t$ □1 $K_2 q_e^2$ □$t\ q_e$	***qe***	1.677
		R^2	0.995
5	Intraparticle diffusion	***c* (mg/g)**	0.196
	$qt = Kpt^{1/2} + c$	R^2	0.946
		***K*p (mg/g·min$^{1/2}$)**	0.143
		R^2	0.977
6	Elovich equation model	***α***	0.214
	$qt = [1/\beta]\ln[\alpha\beta] + [1/\beta]\ln t$		
		***β* (g/mg)**	2.691
7	Natarajan and Khalaf	***K* (min^{-1})**	0.0116
	$\mathrm{Ln}(Co/Ct) = Kt$	R^2	0.915

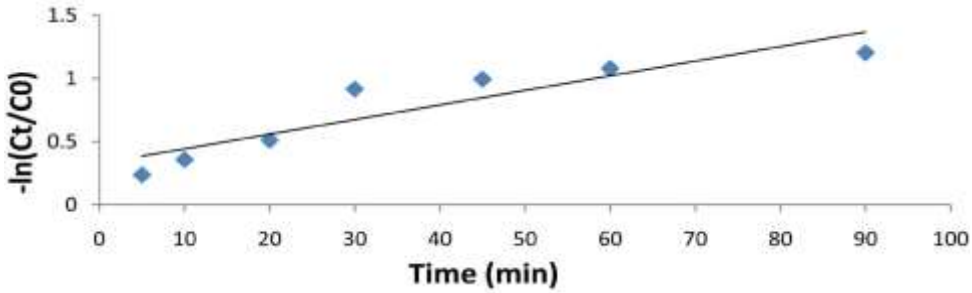

Figure 9. First Order Kinetic Equation plot for the adsorption of iron ions on HApMn.

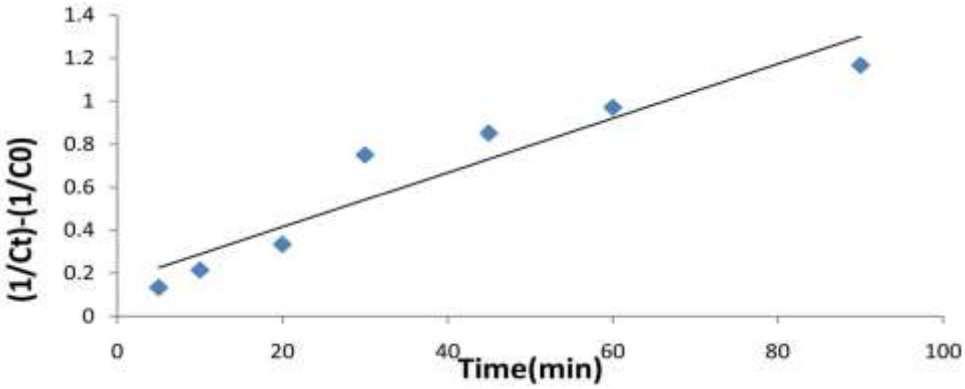

Figure 10. Second order rate equation plot for the adsorption of iron ions on HApMn.

Regression value (*R*2) is greater than 0.9 for iron ions. Indicating that the equa-tion can be applied to experimental data for iron ions.

Pseudo First Order Kinetic Equation

The mathematical relationship to describe the pseudo-motif model proposed by Lagergren is shown in equation [12] [27]:

$$\ln \square q_e - q_t \square \square \ln q_e - K_1 p_t \qquad (7)$$

where *K*1 is the rate constant of pseudo-first order adsorption (L/min). *qe* and *qt* are adsorption capacity (mg/g) at equilibrium and at any time *t*, respectively. The value of the constants *qe*, *k*1 and *R*2 obtained from the linear plot of ln(*qe* − *qt*) vs *t* (**Figure 11**) are shown in **Table 3**. The regression rate *R*2 > 0.9 For iron ions.

Pseudo-Second Order Kinetic Equation

The linear relationship of pseudo-second order kinetic model is given by [12] [23] [24] [25] [27] [28]:

$$t/q_t \square 1/K_2 q_e^2 \square t/q_e \qquad (8)$$

where *K*2 (g/mg/min) is the rate constant of pseudo-second order adsorption rate constant. The values of *k*2, *R*2 and *qe* were calculated from the plots of *t*/*qt* on the vertical axis, and *t* (min) on the horizontal

axis (**Figure 12**) as shown in **Ta-ble 3**. The regression $R2 > 0.9$, for iron meaning that this model provided the best fit for the adsorption data.

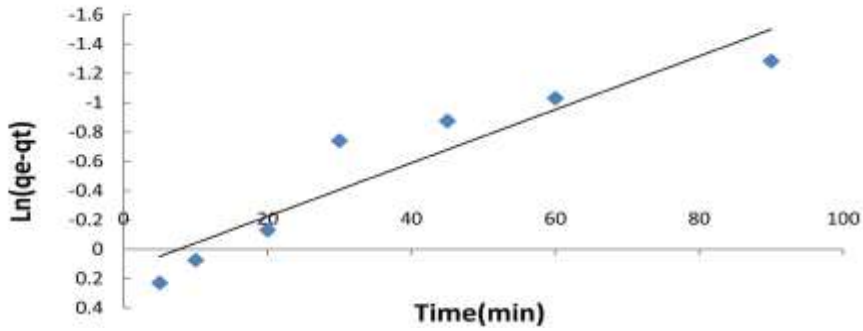

Figure 11. Pseudo first-order kinetic plot for the adsorption of iron ions on HApMn.

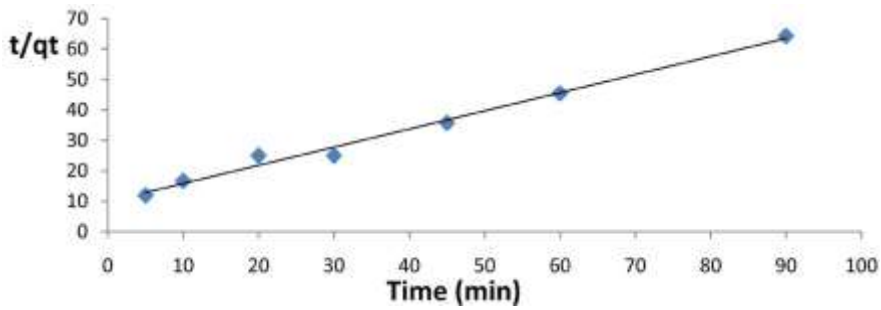

Figure 12. Pseudo second order rate plot for the adsorption of iron ions on HApMn.

Elovich Equation

The Elovich equation used to describe the kinetics of chemisorption of gas on solids, The linear relationship is given by [12] [23] [24] [25] [27] [28]:

$$q_t \; \square \; \square 1 \beta \; \square \ln \; \square \alpha\beta \; \square \; \square \; \square 1 \beta \; \square \ln t \qquad (9)$$

where, the constants α and β were obtained from the slope and intercept of the linear plot of qt (mg/g) against ln(t, min) as shown in (**Figure 13**), for the ad-sorption of iron ions on HApMn.

Intra-Particle Diffusion Rate Equation

The intra-particle diffusion equation [12] [28] [29] [30] is given as Equation (10) shown in **Figure 14**.

$$q_t \; \square \; kp_t^{1\,2} \; \square \; C \qquad (10)$$

where, *Kp* (mg/g·min1/2) is the intraparticle diffusion rate constant and *C* is the intercept. by drawing *qt* on the Y-axis against *t* (min) on X-axis we can find the slope, intercept and correlation coefficient as seen in **Table 3**, it was observed that the intraparticle diffusion rate constant increased with an increase in initial concentrations.

Natarajan and Khalaf

Natarajan and Khalaf equation [31] developed a relationship between the initial concentration and concentration at any time. The linear form is expressed as:

ln □Co Ct □ □ K n · t (11)

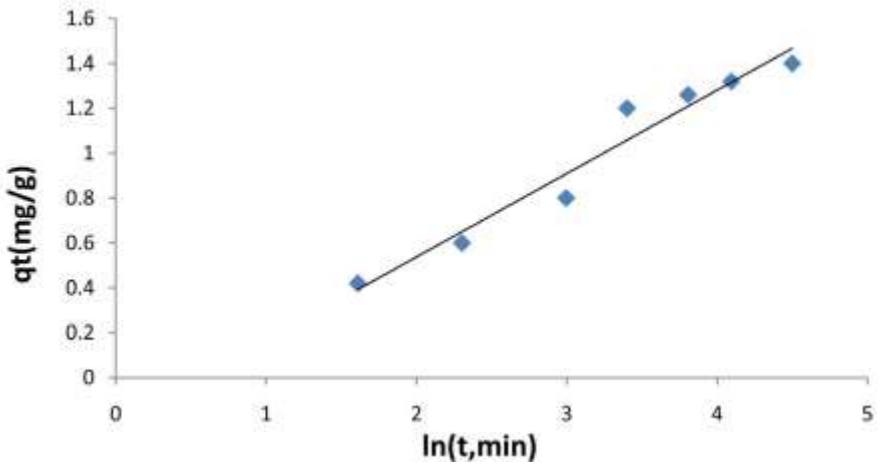

Figure 13. Elovich plot for the adsorption of iron ions on HApMn.

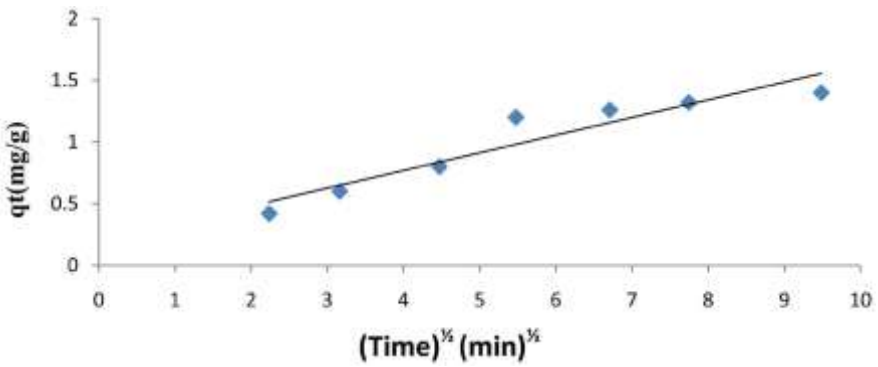

Figure 14. Intraparticle diffusion equation plot for the adsorption of iron ions on HApMn.

where, *Ct* is the concentration of iron (mg/L) at time *t*. The plot of ln(*Co*/*Ct*) against *t* will give a straight line and the value of *kn* can be obtained from the slope of the graph (**Figure 15**). The values

of *kn* and *R*2 are shown in **Table 3**. The correlation coefficient R2 for the pseudo second order kinetic model is greater than 0.99.

Adsorption Isotherms

Adsorption data are generally described by adsorption isotherms, such as Freun-dlich, Langmuir, and Temkin isotherm models.

Freundlich Isotherm

This model proposes monolayer sorption with a heterogeneous energy distribu-tion of active sites, accompanied by interactions between adsorbed molecules. The general form of this model is presented in the following equation [12] [32]:

$$q_e = K_F C_e^{1/n} \quad (12)$$

The linear form of the Equation (12) is [12] [33]:

$$\ln q_e = \ln K_F + \frac{1}{n} \ln C_e \quad (12a)$$

This isotherm relates the amount of solute adsorbed at equilibrium per weight

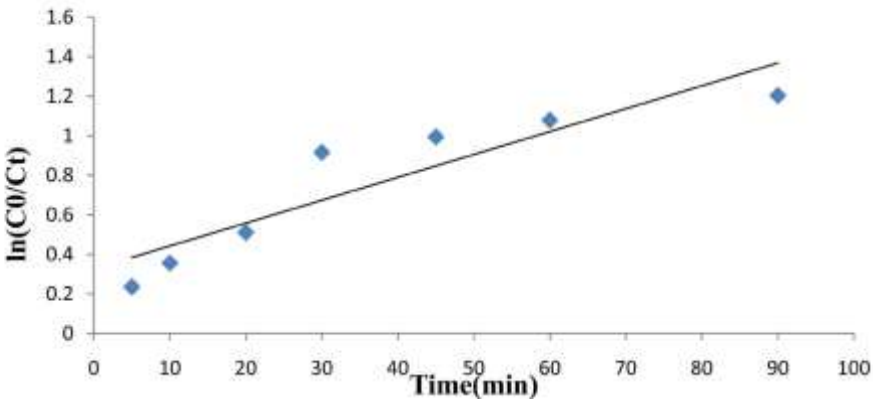

Figure 15. Natarajan and Khalaf plot for the adsorption of iron ions on HApMn.

of adsorbent where *qe* (mol/g) to the adsorbate concentration at equilibrium *Ce* (mol/dm3), is the most widely non-linear sorption models used. *KF* (mg/g) stands for adsorption capacity and 1/*n* stands for adsorption intensity.

By plotting of ln*qe* on Y-axis versus ln*C* on X-axis we can determine *KF* and 1/*n* from a slope and intercept respectively (**Figure 16**).

Langmuir Isotherm

The Langmuir model [8] [26] [29] [32] describes adsorption as a monolayer surface corresponding to solids with identical homogeneous sites. This is ac-cording to the following linear relationship:

$$C_e / q_e = 1/(q_{max} b) + C_e / q_{max} \quad (13)$$

where *qe* is the amount adsorbed (mg/g), *Ce* is the equilibrium concentration of the adsorbate ions (mg/L), *q*max and *b* are Langmuir constants. Where, qmax (mg/g) is Langmuir constant related to maximum adsorption capacity (mono-layer capacity) andb (L/mg) is the energy of adsorption.

By plotting of *Ce*/*qe* versus *Ce* should indicate a straight line of slope 1/*q*max and an intercept of 1/*q*max *b*.

Figure 17: shows Langmuir isotherm for iron ions adsorption at various ini-tial iron ions concentrations using HApMn at adsorbent dosage of 0.1 g, agita-tion speed of 400 rpm, solution pH 6 and temperature of 30˚C. Based on the correlation coefficient (*R*2) shown in **Table 4** the adsorption isotherm can be better described by Langmuir equation. Also, the Langmuir equation yields a better fit of the experimental data than the Freundlich equation. Further, the es-sential characteristics of Langmuir isotherm can be described by a separation factor *RL*, which indicates the shape of the isotherm and nature of the adsorption process. this is expressed by the following equation [8] [29] [30] [34].

$$R_L = 1/(1 + bC_o) \quad (14)$$

where *Co* is the initial concentration of iron ions (mg/L). The separation factor When *RL* is greater than 1, the process is unfavourable, *RL* = 1, Linear, 0 < *RL* < 1, favorable and *RL* = 0 irreversible. In this study, the Calculated values for *RL* are

Table 4. Adsorption isotherms constants.

Freundlich			Langmuir			Temkin		
***Kf* (mg/g)**	**1/*n***	**R^2**	***q*max (mg/g)**	***B* (L/mg)**	**R^2**	***KT* (L/mg)**	***β* (g/mg)**	**R^2**
1.255	−0.222	0.799	0.603	−0.837	0.958	0.002	−0.201	−0.853

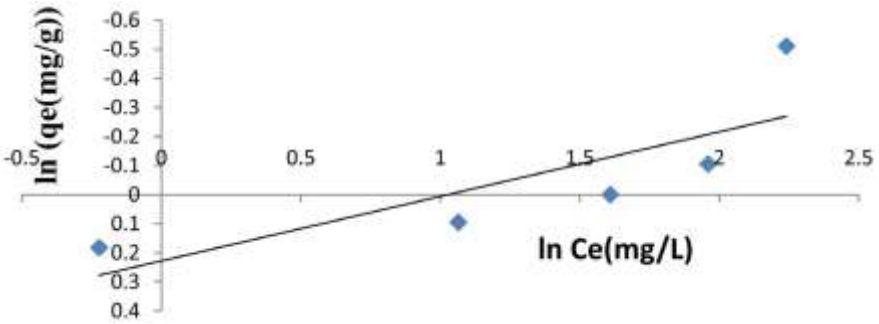

Figure 16. Freundlich isotherm for iron ions sorption on HApMn.

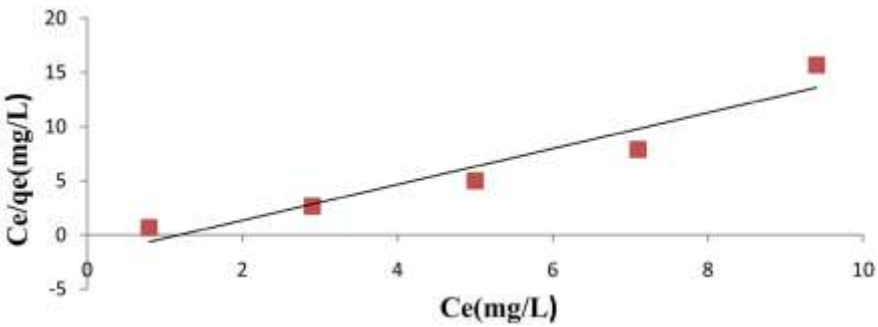

Figure 17. Langmuir isotherm for iron ions adsorption on HApMn.

found to be a fraction in the range of 0 - 1 (0.442), an indication that the adsorp-tion process is favorable [35].

Temkin Isotherm

The linear form of the Temkin equation is given by [8] [29] [30] [36]:

$$q_e \square \beta \ln KT \square \beta \ln C_e \quad (15)$$

where, β which is related to the heat of adsorption, and KT (L/mg) is the equili-brium binding constant corresponding to the maximum binding energy. By plotting qe on Y-axis versus on X-axis we can be calculated β and KT calculated from the slope and the intercept. **Figure 18**: shows Temkin model isotherm for iron ions adsorption at various initial iron ions concentrations using HApMn at adsorbent dosage of 0.1 g, agitation speed of 400 rpm, solution pH 6 and tem-perature of 25˚C.

Thermodynamic Parameters

Thermodynamic parameters [37] such as and entropy (ΔS), enthalpy (ΔH) and free energy (ΔG) were determined using Equations (16)-(19)

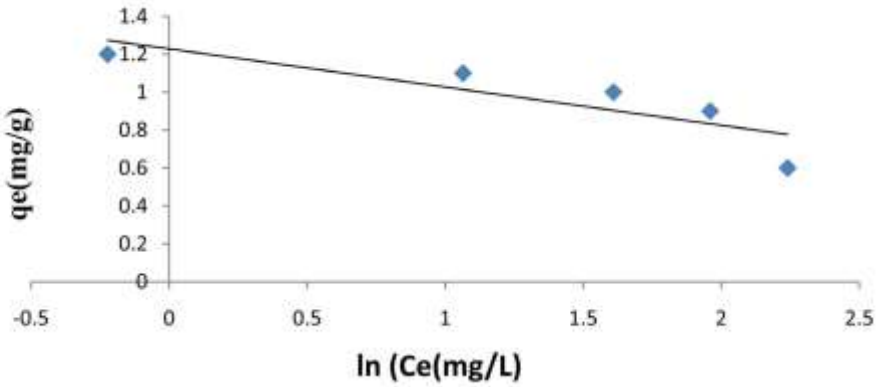

Figure 18. Temkin model plot for Adsorption of iron on HApMn.

$$K_c = q_e - C_e \quad (16)$$

$$\Delta G = -RT \ln K_c \quad (17)$$

$$\ln K_c = \frac{-\Delta H}{R}\left(\frac{1}{T}\right) + \frac{\Delta S}{R} \quad (18)$$

where qe is the amount of solute adsorbed on the adsorbent cubic decimetre of the solution at equilibrium, Kc is the equilibrium constant, and Ce (mol/dm3) is the equilibrium concentration of the solute in solution, T is the temperature in Kelvin and R (8.314 J/K/mol) is the gas constant. By plotting of on Y-axis against1/T on X-axis we found H and S were obtained from the slope and intercept of Vant Hoff isotherm (Figure 19). Table 5 shows the calculated values of the thermodynamic parameters. In order to understand this process better, we must calculate the entropies and enthalpies of temperature periods using the previous equations [32] [38]:

$$\Delta G = \Delta H - T\,\Delta S \quad (19)$$

where, Kc1 is the equilibrium constant at temperature T1 and Kc2 are the equilibrium constant at temperature T2.Increasing the value of G° with increasing temperature leads to the process

of adsorption of iron ions on HApMn become preferred in low temperatures. The negative value of H˚ proves that the adsorption process was exothermic reaction and a certain amount of heat developed during the iron ions that adsorbed on the surface of the adsorbents. The more negative value ofS˚, themore degree of randomization in the solid/liquid interface during the absorption process where entropy expresses the amount of randomness or disorder in the system. We used entropy (ΔS˚) to determine the degree of disorder or random-ness in the system. We know that the higher the negative values of S˚, the low-er the degree of randomization in the solid/liquid interface during the adsorption process [39]. The values of H˚ and S˚ calculated from the plot of lnK versus 1/T.The value of H˚ was negative, indicating that the adsorption reaction was exothermic (high heat of adsorption). Another equation that has been used to

determine the possible adsorption mechanism is the **Dubinin-Radushkevick**

Table 5. Thermodynamic parameters for adsorption of iron ions on HApMn.

T (*K*)	*Kc*	Δ*G* (kg/mol)	Δ*H*	Δ*S*	R^2
298	1.5	0.405			
318	0.379	−0.969	−51	−142	0.991
333	0.200	−1.609			
348	0.127	−2.605			

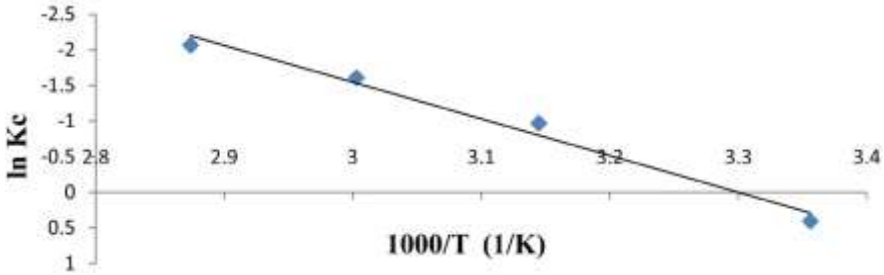

Figure 19. Thermodynamic model plot for Adsorption of iron ions on HApMn.

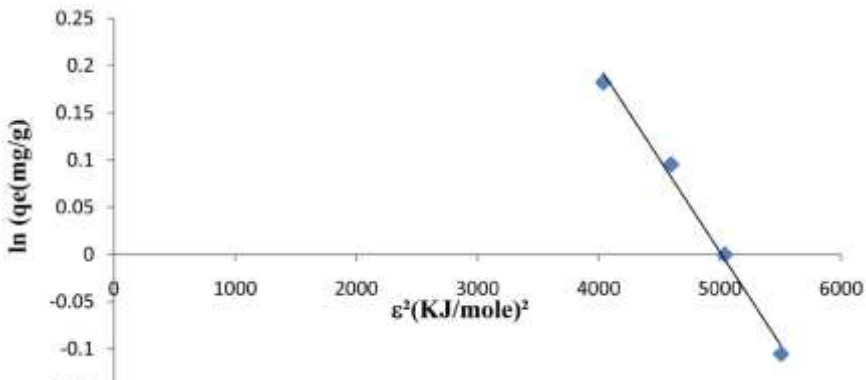

Figure 20. Dubinin-Radushkevick equation plot.

equation, which assumes a constant sorption potential. The linear presenta-tion of this equation is expressed by

$$\ln q_e = \ln q_m - K_E \varepsilon^2 \quad (20)$$

$$\varepsilon = RT \ln \left(1 + \frac{1}{C_e}\right) \quad (21)$$

where ε is the Polanyi potential, *qt* is the monolayer capacity (mol/g), *Ce* is the equilibrium concentration (mol/dm3), and *KE* is the constant related to sorption energy (mol2/KJ2) The parameters *qt* and *KE* can be obtained from the intercept and slope of the plot as shown in **Figure 20**. The free energy of sorption (*E*) is calculated by

$$E = \left(\frac{1}{-2K_E}\right)^{1/2} \quad (22)$$

Adsorption type could be estimated by evaluating of *E* value. If this value is < 8, 8 - 16 or >16 kJ/mol, the adsorption type can be explained by physical adsorption, ion-exchange, or chemical adsorption, respectively [41]. In this case, the
adsorption is chemical adsorption at all temperatures because *E* value was 50 kJ/mol.

CONCLUSION

In this article, we use Modified HApMn for removing iron ions from ground-water. Adsorption of iron on HApMn follows pseudo-second order kinetic model, Langmuir adsorption isotherm, Adsorption capacity from the Langmuir model is 0.604 mg/g, the adsorption process is chemical type because adsorption energy value is 50 kJ/mol, and adsorption is favourable at low temperatures, the negative value of H° confirms that the sorption process is exothermic in nature and a given amount of heat is evolved during the binding iron ions on the surface of adsorbents.

References

[1] Hossain, D., Islam, M.S., Sultana, N. and Tusher, T.R. (2013) Assessment of Iron Contamination in Groundwater at Tangail Municipality, Bangladesh. *Journal of Environmental Science and Natural Resources*, **6**, 117-121. https://doi.org/10.3329/jesnr.v6i1.22051

[2] Prentice, A.M., *et al.* (2017) Dietary Strategies for Improving Iron Status: Balancing Safety and Efficacy. *Nutrition Reviews*, **75**, 49-60. https://doi.org/10.1093/nutrit/nuw055

[3] Abdennebi, N., Benhabib, K., Goutaudier, C. and Bagane, M. (2017) Removal of Aluminium and Iron Ions from Phosphoric Acid by Precipitation of Orga-no-Metallic Complex Using Organophosphorous Reagent. *Journal of Materials and Environmental Science*, **8**, 557-565.

[4] Dubey, S., Banerjee, S., Upadhyay, S.N. and Sharma, Y.C. (2017) Application of Common Nano-Materials for Removal of Selected Metallic Species from Water and Wastewaters: A Critical Review. *Journal of Molecular Liquids*, **240**, 656-677. https://doi.org/10.1016/j.molliq.2017.05.107

[5] Hosseini, H., Rezaei, H., Shahbazi, A. and Maghsudlu, A. (2016) Application of Nano-Lignocellulose for Removal of Nickel Ions from Aqueous Solutions. *Envi-ronmental Resource Research*, **4**, 213-229.

[6] Piuleac, C.G., Sáez, C., Cañizares, P. and Curteanu, S. (2012) Hybrid Model of a Wastewater-Treatment Electrolytic Process. *International Journal of Electrochemi-cal Science*, **7**, 6289-6301.

[7] Mondal, P., Majumder, C.B. and Mohanty, B. (2008) Effects of Adsorbent Dose, Its Particle Size and Initial Arsenic Concentration on the Removal of Arsenic, Iron and Manganese from Simulated Ground Water by Fe3+ Impregnated Activated Carbon. *Journal of Hazardous Materials*, **150**, 695-702. https://doi.org/10.1016/j.jhazmat.2007.05.040

[8] Javadian, H., Ghorbani, F., Tayebi, H. and Asl, S.H. (2015) Study of the Adsorption of Cd (II) from Aqueous Solution Using Zeolite-Based Geopolymer, Synthesized from Coal Fly Ash; Kinetic, Isotherm and Thermodynamic Studies. *Arabian Journal of Chemistry*, **8**, 837-849. https://doi.org/10.1016/j.arabjc.2013.02.018

[9] Agarwal, S., *et al.* (2016) Efficient Removal of Toxic Bromothymol Blue and Methy-lene Blue from Wastewater by Polyvinyl Alcohol. *Journal of Molecular Liquids*, **218**, 191-197. https://doi.org/10.1016/j.molliq.2016.02.060

[10] Bhatnagar, A. and Sillanpää, M. (2017) Removal of Natural Organic Matter (NOM) and Its Constituents from Water by Adsorption—A Review. *Chemosphere*, **166**, 497-510. https://doi.org/10.1016/j.chemosphere.2016.09.098

[11] Mrinal, D.D., Adak, K., Mondal, B., Dhak, P. and Sen, S. (2017) A Comparative Study on Fluoride Removal Capacity from Drinking Water by Adsorption Using Nano-Sized Alumina and Zirconia Modified Alumina Prepared by Chemical Route. *Advances in Water Science and Technology*, **4**, 1-10.

[12] Abuh, M.A., Akpomie, G.K., Nwagbara, N.K., Abia-Bassey, N., Ape, D.I. and Aya-bie, B.U. (2013) Kinetic Rate Equations Application on the Removal of Copper (II) and Zinc (II) by Unmodified Lignocellulosic Fibrous Layer of Palm Tree Trunk-Single Component System Studies. *International Journal of Basic and Ap-plied Sciences*, **50**, 800-809.

[13] Elhafez, S.E.A., Hamad, H.A., Zaatout, A.A. and Malash, G.F. (2017) Management of Agricultural Waste for Removal of Heavy Metals from Aqueous Solution: Ad-sorption Behaviors, Adsorption Mechanisms, Environmental Protection, and Techno-Economic Analysis. *Environmental Science and Pollution Research*, **24**, 1397-1415. https://doi.org/10.1007/s11356-016-7891-7

[14] Voisin, H., Bergström, L., Liu, P. and Mathew, A. (2017) Nanocellulose-Based Materials for Water Purification. *Nanomaterials*, **7**, 57. https://doi.org/10.3390/nano7030057

[15] Bhadra, B.N., Ahmed, I., Kim, S. and Jhung, S.H. (2017) Adsorptive Removal of Ibuprofen and Diclofenac from Water Using Metal-Organic Framework-Derived Porous Carbon. *Chemical Engineering Journal*, **314**, 50-58. https://doi.org/10.1016/j.cej.2016.12.127

[16] Wang, X., Liang, Y., An, W., Hu, J., Zhu, Y. and Cui, W. (2017) Removal of Chro-mium (VI) by a Self-Regenerating and Metal Free g-C3N4/Graphene Hydrogel Sys-tem via the Synergy of Adsorption and Photo-Catalysis under Visible Light. *Applied Catalysis B*: *Environmental*, **219**, 53-62. https://doi.org/10.1016/j.apcatb.2017.07.008

[17] Sarker, M., Bhadra, B.N., Seo, P.W. and Jhung, S.H. (2017) Adsorption of Benzotriazole and Benzimidazole from Water over a Co-Based Metal Azolate Framework MAF-5(Co). *Journal of Hazardous Materials*, **324**, 131-138. https://doi.org/10.1016/j.jhazmat.2016.10.042

[18] Elkady, M.F., Mahmoud, M.M. and Abd-El-Rahman, H.M. (2011) Kinetic Approach for Cadmium Sorption Using Microwave Synthesized Nano-Hydroxyapatite. *Journal of*

Non-Crystalline Solids, **357**, 1118-1129. https://doi.org/10.1016/j.jnoncrysol.2010.10.021

[19] Gotić, M., Jurkin, T., Musić, S., Unfried, K., Sydlik, U. and Bauer-Šegvić, A. (2013) Microstructural Characterizations of Different Mn-Oxide Nanoparticles Used as Models in Toxicity Studies. *Journal of Molecular Structure*, **1044**, 248-254. https://doi.org/10.1016/j.molstruc.2012.09.083

[20] Abdel Ghafar, H.H., Ali, G.A.M., Fouad, O.A. and Makhlouf, S.A. (2015) Enhance-ment of Adsorption Efficiency of Methylene Blue on Co3O4/SiO2 Nanocomposite. *Desalination and Water Treatment*, **53**, 2980-2989. https://doi.org/10.1080/19443994.2013.871343

[21] Hamdaoui, O. (2017) Adsorption of Cu(II) from Aqueous Phase by Cedar Bark.*Journal of Dispersion Science and Technology*, **38**, 1087-1091. https://doi.org/10.1080/01932691.2016.1225261

[22] Bagdadee A.H, “Imitation intellect Techniques Implement for Improving Power Quality in Supply Network ,IEEE International conference on Signal Processing, Communication, Power and Embedded System (SCOPES)-2016 DOI:10.1109/SCOPES.2016.7955611

[23] A.H Bagdadee “To reduce impact of the variation of power from renewable energy by using super capacitor in Smart grid ,WSEAS TRANSACTIONS on POWER SYSTEMS Vol.11 2016,USA.

[24] A.H.Bagdadee, 'Rural Electrification Through Micro-grid in Bangladesh' .Oxford Academic Studies Press (OASP) in Engineering Sciences and TechnologyJournal (ESTJ). Vol. 10 Issue 5. ISSN: 1465-2382, 2015.UK

[25] Amam Hossain Bagdadee , Md. Bayezid Islam “TO IMPROVE POWER FAILUREANDPROTECT SUSTAINABILITY OF THE ENVIRONMENT IN BANGLADESH BY THERENEWABLE ENERGY” International Journal of Energy and Environmental Research Vol.3, No.1, pp.29-42, ISSN: 2055-0200,March 2015.UK

[26] A.HBagdadee ,Nazib Sobhan “Developing model of control stratagem with variable speed drive by synchronous speed in micro-Hydro plant” Published in International Journal of Power and Renewable Energy Systems (IJPRES)Vol.2,2015PP.88-100 ISSN 2374-376X.USA

[27] Amam Hossain Bagdadee,“ ASSESSMENT OF PV OPERATION IN BANGLADESH, International Journal of Energy and Environmental Research Vol.2, No.1, ISSN: 2055-0200,March 2014.UK

[28] Bagdadee, AH “Status and Reform towards Development Energy Sector of Bangladesh” European Journal of Advances in Engineering and Technology, Vol. 2(2): 24-28 ISSN: 2394 - 658X,2015.India

[29] A.H,Bagdadee,Abu Salman ShaikatPROPERTY OF ANCILLARY SERVICE MARKETS ON FREQUENCY CONTROL PERFORMANCE OF POWER SYSTEMS,International Journal of Engineering and Advance Technology Studies Vol.2, No.3, ISSN: 2053-5791,2014.UK

[30] A.H Bagdadee, Sheikh Aminur Rahaman ASSESSMENT OF CLIMATE CHANGE WITH ENERGY EXPANSION FOR DEVELOPING COUNTRIES ,International Journal of Energy and Environmental Research Vol.3, No.2 ISSN 2055-0200,UK

[31] Bagdadee, A.H. & Zhang, L. J. Electr. Eng. Technol. (2019) 14: 1841. https://doi.org/10.1007/s42835-019-00220-y

[32] Ioannou, Z. and Simitzis, J. (2009) Adsorption Kinetics of Phenol and 3-Nitrophenol from Aqueous Solutions on Conventional and Novel Carbons. *Journal of Hazard-ous Materials*, **171**, 954-964. https://doi.org/10.1016/j.jhazmat.2009.06.0